

1 **Application of Material Balance Methods to CO₂ Storage Capacity Estimation within**
2 **selected Depleted Gas Reservoirs**

3
4 A. L. Clarke^{1*}, J. Imber², R. J. Davies³, J. van Hunen², S. E. Daniels⁴, G. Yielding⁵

5
6 ¹*Department of Earth Sciences, Durham University, Durham, DH1 3LE, UK. Presently at*
7 *Badley Geoscience Ltd., Spilsby, Lincolnshire, PE23 5NB, UK.*

8 ²*Department of Earth Sciences, Durham University, Durham, DH1 3LE, UK.*

9 ³*Department of Earth Sciences, Durham University, Durham, DH1 3LE, UK. Presently at*
10 *Executive Office, Newcastle University, Newcastle upon Tyne, NE1 7RU, UK.*

11 ⁴*Geospatial Research Ltd., Department of Earth Sciences, Durham University, Durham, DH1*
12 *3LE, UK.*

13 ⁵*Badley Geoscience Ltd., Spilsby, Lincolnshire, PE23 5NB, UK*

14 *Corresponding author (e-mail: amy@badleys.co.uk)

15
16 **Abstract:** Depleted gas reservoirs are potential sites for CO₂ storage, therefore it is important
17 to evaluate their storage capacity. Historically, there have been difficulties identifying the
18 reservoir drive mechanism of gas reservoirs using traditional P/z plots, having direct impacts
19 for estimation of the OGIP and dependent parameters for both theoretical and effective CO₂
20 storage capacity estimation. Cole plots have previously provided an alternative method of
21 characterisation, being derived from the gas material balance equation. We use production
22 data to evaluate the reservoir drive mechanism in four depleted gas reservoirs (Hewett Lower
23 Bunter, Hewett Upper Bunter and North and South Morecambe) on the UK continental shelf.
24 Cole plots suggest the North Morecambe and Hewett Upper Bunter reservoirs experience
25 moderate water drive. Accounting for cumulative water influx into these reservoirs, the
26 OGIP decreases by up to 20% compared with estimates from P/z plots. The revised OGIP
27 values increase recovery factors within these reservoirs, hence, geometrically-based
28 theoretical storage capacity estimates for the North Morecambe and Hewett Upper Bunter
29 reservoirs increase by 4% and 30%, respectively. Material balance approaches yield more
30 conservative estimates. Effective storage capacity estimates are between 64-86% of
31 theoretical estimates within the depletion drive reservoirs, and 53-79% within the water drive
32 reservoirs.

33
34 **Supplementary material:** A more detailed description of the aquifer modelling is available
35 at: <http://www.geolsoc.org.uk/>

36
37 Carbon dioxide capture and storage (CCS) is an important technology to mitigate the effect of
38 CO₂ emissions on climate (Holloway 2009), with at least 22 large-scale CCS projects in
39 operation or construction globally, capturing approximately 40 MtCO₂ per annum (Global
40 CCS Institute 2015). The UK is predicted to rely upon fossil fuel combustion for energy
41 generation for at least the next few decades (Holloway *et al.* 2006). As such, depleted gas
42 fields on the UK continental shelf have been under consideration for CO₂ storage, offering a
43 storage capacity of ca. 6100 Mt CO₂ (Holloway 2009), substantially larger than that of
44 depleted UK oil reservoirs. In comparison to alternative CO₂ storage sites, such as
45 unmineable coal seams and saline aquifers, the dynamic behaviour of depleted gas reservoirs
46 is well understood and a wealth of data exists for most reservoirs spanning their entire
47 productive lifetimes. In particular, the UK Triassic Sherwood Sandstone Group (alias,
48 Bunter Sandstone Formation (Johnson *et al.* 1994)) is considered for CO₂ storage, being a
49 major sandstone unit with many of the necessary basic characteristics, including structural
50 traps (such as anticlines), good porosity and permeability, large storage capacities and good

51 lateral and vertical seal. Three of the largest depleted Triassic gas fields on the UK
52 continental shelf are the Hewett Gas Field of the Southern North Sea, and the South and
53 North Morecambe Gas Fields of the East Irish Sea Basin.

54

55 The CO₂ storage capacity of a depleted gas reservoir is dependent on the pressure and
56 compressibility of the residual fluids (including gas and water) occupying the pore space. As
57 such, it is necessary to establish whether a gas reservoir experiences a water drive, and if so,
58 attempt to quantify the volume of water influx into the reservoir throughout its productive
59 lifetime. Usually, the P/z plot (reservoir pressure divided by the gas compressibility factor) is
60 used to identify the reservoir drive mechanism, i.e. establish whether a gas reservoir
61 experiences a water drive (Vega & Wattenbarger 2000). However, it has been documented
62 extensively within the literature that P/z plots are notoriously difficult to solve within water
63 drive reservoirs (Agarwal *et al.* 1965, Bruns *et al.* 1965, Chierici *et al.* 1967, Dake 1978,
64 Hagoort 1988, Pletcher 2002, Vega & Wattenbarger 2000). The insensitivity of the P/z plot,
65 particularly within a water drive reservoir, can result in misinterpretation of the reservoir
66 drive mechanism and a significant overestimation of the original gas in place (OGIP) (Vega
67 & Wattenbarger 2000). Several published methods used to estimate CO₂ storage capacity
68 rely on either direct estimation of the OGIP, or a parameter that is dependent upon the OGIP
69 (such as the recovery factor). Therefore, it is important to obtain a precise value for the
70 OGIP to estimate CO₂ storage capacity.

71

72 The aim of this study is to use production data and material balance methods to estimate the
73 theoretical and effective CO₂ storage capacities in four depleted gas reservoirs with well-
74 constrained production histories and contrasting drive mechanisms. The objectives are to: (1)
75 compare the theoretical and effective storage capacity estimates predicted by different
76 published analytical approaches (Bachu *et al.* (2007); Holloway *et al.* (2006); Tseng *et al.*
77 (2012)); (2) evaluate the impact of aquifer influx on theoretical and effective storage capacity
78 estimates for water drive reservoirs; and (3) identify which methods yield the most
79 conservative theoretical storage capacity estimates for depletion and water drive reservoirs.

80

81 Specifically, we use production and pressure data from the Hewett, South Morecambe and
82 North Morecambe gas fields to demonstrate the use of material balance methods in CO₂
83 storage capacity estimation. Production data are interpreted using both P/z plots and Cole
84 plots (Cole 1969, Pletcher 2002) to establish reservoir drive mechanism. This approach is
85 taken due to the cumulative volume of produced water being unknown for these reservoirs
86 across their productive lifetimes. For depletion drive reservoirs, OGIP is estimated via linear
87 extrapolation of the trend on the P/z plot down to the x-axis (y=0). For water drive
88 reservoirs, an alternative methodology is used to model aquifer performance throughout the
89 productive lifetime and to estimate the cumulative volume of water influx (W_e) into the
90 reservoirs analysed. Once a reasonable estimate is obtained for W_e , the value can be used to
91 calculate the OGIP. The OGIP estimates from depletion drive and water drive gas reservoirs
92 can then be used to estimate both the theoretical and effective CO₂ storage capacities.

93

94 It is important to note that this paper uses published methods to analyse the data from the four
95 reservoirs and is, therefore, bound to the limitations of those methods. Certain approaches,
96 such as the use of the Cole plot, have been taken in the case of the water drive reservoirs (the
97 Hewett Upper Bunter Sandstone and North Morecambe Sherwood Sandstone reservoirs) as
98 there is a lack of water production data from them. As such, this paper represents an attempt
99 at comparing estimates of CO₂ storage capacities using published material balance methods.

100

101 Our results for the Hewett field (Fig. 1) have been derived from published data (e.g. Cooke-
102 Yarborough & Smith 2003), and from historic field production and pressure datasets kindly
103 provided by Eni Hewett Limited, and which are already in the public domain (Clarke et al.
104 2010). Results for the Morecambe fields (Fig. 2) are derived from historic field production
105 and pressure datasets kindly provided by Centrica. We emphasise that our results for the
106 Hewett field are entirely our own, and do not constitute interpretations or views of Eni
107 Hewett Ltd. or its partner, Perenco UK (Gas) Ltd. Similarly, our results for the South and
108 North Morecambe fields are entirely our own, and do not constitute interpretations or views
109 of Centrica.

110

111 **Definition of “Storage Capacity”**

112

113 The theoretical CO₂ storage capacity is a maximum upper limit to a capacity estimate, which
114 often represents the entire pore space of the storage complex, or the pore space with known
115 displaceable resident fluids (Bachu *et al.* 2007). Alternatively, theoretical CO₂ storage
116 capacity may be defined as the mass of CO₂ injected from abandonment pressure to initial
117 reservoir pressure, to occupy the pore volume of gas produced (Tseng *et al.* (2012)).

118 Effective storage applies technical (geological and engineering) limitations to the theoretical
119 storage capacity estimate (Bachu *et al.* 2007). In this study, effective storage capacity refers
120 to the available pore space taking account of any residual hydrocarbons and cumulative water
121 influx, assuming the overall pore volume is unchanged during gas production and CO₂
122 injection (Tseng *et al.* (2012)).

123

124 **Geological Background**

125

126 The Triassic Sherwood Sandstone Group is a major sandstone unit with many of the basic
127 characteristics necessary for CO₂ storage including structural traps (such as anticlines), good
128 porosity and permeability, large storage capacities and a good lateral and vertical seal
129 provided by the overlying Mercia Mudstone Group, a proven hydrocarbon seal (Bentham
130 2006, Brook *et al.* 2003, Kirk 2006). Many of its structural anticlines occur at depths of at
131 least 800m, therefore injected CO₂ may be stored in the supercritical phase assuming a
132 geothermal gradient of 25°C/km.

133

134 ***The Hewett Gas Field***

135

136 The Hewett Gas Field is the second largest UK North Sea gas field and the third largest UK
137 gas field. It is located 16 km NE of Bacton on the Norfolk coastline, one of the most
138 proximally situated gas fields on the UK continental shelf (Fig. 1). The Hewett Gas Field
139 comprises three major reservoirs: the Triassic Upper and Lower Bunter Sandstone
140 Formations (alias Sherwood Sandstone Group (Johnson *et al.* 1994, Warrington *et al.* 1980)),
141 and the Permian Zechsteinkalk reservoir (Fig. 1). The Permian reservoir is not considered
142 here for carbon storage due to its complex compartmentalisation (Cooke-Yarborough &
143 Smith 2003) which is poorly understood, and therefore it would be too expensive and high-
144 risk to develop (Bentham 2006).

145

146 The Hewett Upper and Lower Bunter Sandstone reservoirs define NW-SE oriented anticlines,
147 parallel to the original Hercynian structural trend (Fig. 1). The South Hewett Fault and
148 Dowsing Fault Zone are reactivated Hercynian faults (Cooke-Yarborough & Smith 2003) but
149 do not act to structurally close the Bunter reservoirs of the Hewett Gas Field.

150

151 The Hewett Lower Bunter structural anticline is four-way dip-closed. The Bunter Shale
152 Formation of the Bacton Group forms the direct cap rock to the reservoir, and within the
153 Hewett Field maintains an almost constant thickness averaging 230 m. The stratigraphically
154 higher Upper Bunter Sandstone structural anticline is three-way dip-closed to the north, south
155 and west. It is closed by the North Hewett Fault on the central-eastern flank. The Dowsing
156 Dolomitic Formation of the Haisborough Group forms the direct cap rock to the reservoir,
157 with an average thickness of 163 m over much of the Hewett anticline, thinning towards the
158 south-east to an average of 104 m. There is greater than 600 m of overburden above the
159 Dowsing Dolomitic Formation, consisting of the remaining formations of the Haisborough
160 Group, the Penarth Group and the Lias Group, all of which are likely to act as secondary
161 seals.

162

163 Production began from the Hewett Lower Bunter Sandstone reservoir in 1969, and later from
164 the Hewett Upper Bunter Sandstone reservoir in 1973. The two reservoirs contained gas of
165 strikingly different compositions, with the Hewett Upper Bunter reservoir containing
166 significant quantities of hydrogen sulphide (Cooke-Yarborough & Smith 2003); evidence to
167 suggest the reservoirs are entirely separate from each other. Further evidence for this has
168 been proven from production and pressure data gathered throughout their productive
169 lifetimes, with a substantial pressure drop in the Hewett Lower Bunter Sandstone reservoir
170 following the onset of production having no effect on the initial reservoir pressure of the
171 Hewett Upper Bunter Sandstone reservoir (Fig. 3). The reservoirs also have different initial
172 reservoir pressures and gas-water-contacts.

173

174 Both reservoirs consist of clean, braided fluvial and sheetflood sandstones with a high
175 reservoir quality although there is a degree of heterogeneity, particularly with respect to
176 permeability. In the Hewett Lower Bunter Sandstone reservoir, the interquartile range of
177 porosity data is between 11.8% - 24.0 % with a median of 18.1%, and permeability data is
178 between 14.5 – 1043.4 mD with a median of 195.5 mD. In the Hewett Upper Bunter
179 Sandstone reservoir, the interquartile range of porosity data is between 15.7 – 24.2 % with a
180 median of 20.1 %, and permeability data is between 43.0 – 907.5 mD with a median of 262.4
181 mD. Production has been straightforward in the Hewett Lower Bunter Sandstone reservoir
182 with a recovery factor exceeding 96 % (Cooke-Yarborough & Smith 2003). The Hewett
183 Upper Bunter has experienced recovery losses as a result of significant aquifer influx into the
184 reservoir, but overall recovery factors are expected to exceed 90 % (Cooke-Yarborough &
185 Smith 2003). The reservoir was at risk of watering out, however following the onset of
186 production from the neighbouring Little Dotty Upper Bunter Sandstone reservoir, which
187 shares the Bunter aquifer, water influx slowed substantially (Cooke-Yarborough & Smith
188 2003). From Fig. 3 it is possible to observe a pre-production pressure drop in the Little Dotty
189 Upper Bunter Sandstone reservoir as a result of production from the Hewett Upper Bunter
190 Sandstone reservoir.

191

192 *The Morecambe Gas Fields*

193

194 The South Morecambe Gas Field is the second largest UK gas field and is located 32 miles
195 west of Blackpool (Kirk 2006). The North Morecambe Gas Field is again of significant
196 capacity (but smaller than South Morecambe) and is situated just to the north, separated from
197 the South Morecambe Gas Field by a NE-SW trending graben (Fig. 2). Both North and
198 South Morecambe contain Triassic gas producing reservoirs of the Sherwood Sandstone
199 Group.

200

201 The South Morecambe Sherwood Sandstone reservoir is a structural anticline consisting of a
202 northern limb, which is fault bounded to the north, west and east, and a southern limb, which
203 is fault bounded to the west and dip-closed to the east (Stuart & Cowan 1991), (Fig. 2). The
204 North Morecambe Sherwood Sandstone reservoir is a N-S trending, north-westerly dipping
205 fault block, fault bound to the east, west and south, but dip-closed to the north (Stuart 1993),
206 (Fig. 2).

207
208 The South Morecambe Sherwood Sandstone reservoir has ca. 670 m of overlying sealing
209 units (Bastin *et al.* 2003), and North Morecambe, ca. 899 m (Cowan & Boycott-Brown
210 2003), consisting of the Mercia Mudstone Group, Penarth Group and Lias Group. A narrow
211 graben separates the South and North Morecambe Gas Fields. The graben's two bounding
212 faults are considered to be full seals: the faults have substantial throws along them meaning
213 the reservoirs will be juxtaposed against top seal. The reservoirs also have different reservoir
214 pressures (Fig. 4), gas compositions and gas-water-contacts. There has been no evidence for
215 pressure communication between the two reservoirs over their productive lifetimes (Fig. 4).
216 North Morecambe has several small faults within the reservoir, however, the only significant
217 internal fault has a 30 m maximum throw and defines an easterly fault terrace which is in
218 pressure communication with the remainder of the reservoir (Cowan & Boycott-Brown
219 2003).

220
221 Both reservoirs consist of fluvial (braided stream and sheetflood) sandstones (Stuart &
222 Cowan 1991). The main control on reservoir properties and performance is governed by
223 authigenic platy illite abundance and distribution. Platy illite was originally precipitated
224 beneath a palaeo-gas-water-contact (Bastin *et al.* 2003). In the illite-free zone the reservoirs
225 enjoy relatively good reservoir properties with reasonably high porosity and permeability
226 values despite a degree of heterogeneity. However, in the illite-affected zone, permeability
227 can be reduced by up to two orders of magnitude (Stuart 1993).

228
229 In the illite-free zone of the South Morecambe Sherwood Sandstone reservoir, the
230 interquartile range of porosity data is between 7.8 – 14.3 % with a median of 10.8 %, and
231 permeability data is between 0.3 – 28.9 mD with a median of 2.8 mD. In the illite-affected
232 zone, interquartile range of porosity data is between 10.7 – 16.5 % with a median of 13.6 %,
233 and permeability data is between 0.2 – 8.5 mD with a median of 1.2 mD.

234
235 Likewise, in the illite-free zone of the North Morecambe Sherwood Sandstone reservoir, the
236 interquartile range of porosity data is between 11.6 – 17.7 % with a median of 14.7 %, and
237 permeability data is between 6.5 – 287.5 mD with a median of 64.0 mD. In the illite-affected
238 zone, the interquartile range of porosity data is between 7.5 – 13.0 % with a median of 10.0
239 %, and permeability data is between 0.05 – 2.2 mD with a median of 0.3 mD – greatly
240 reduced due to the presence of illite.

241
242 Despite this, production from the illite-free zone has been successful with recovery factors of
243 93 % in South Morecambe and 80 % in North Morecambe.

244 245 **Distinguishing Reservoir Drive Mechanism and Estimating the OGIP**

246
247 Material balance, or the P/z plot, is a popular method used to establish the presence (or
248 absence) of a water drive within producing gas reservoirs and estimate the OGIP (Agarwal *et al.*
249 1965, Archer & Wall 1986, Bruns *et al.* 1965, Chierici *et al.* 1967, Dake 1978, Hagoort
250 1988, Pletcher 2002, Vega & Wattenbarger 2000). The material balance equation is

251 particularly suited to true depletion drive (volumetric) reservoirs, i.e. reservoirs that
 252 experience no water encroachment throughout their productive lifetime and no reservoir
 253 compaction. As such, the initial gas volume at the initial reservoir pressure is equal to the
 254 remaining gas volume at lower pressure (Archer & Wall 1986). Hence,

$$G(B_{gi}) = (G - G_p)B_g \quad (1)$$

256 where, G is the original gas in place, B_g is the gas formation volume factor (reservoir
 257 volume/standard condition volume), G_p is the cumulative volume of produced gas, and the
 258 subscript, i , denotes initial reservoir conditions (after Archer & Wall (1986)).

260 The gas formation volume factor (B_g) is a ratio between reservoir and standard condition
 261 volumes. Therefore, the real gas equation of state ($PV = znRT$) can be substituted. In an
 262 isothermal reservoir (where the initial reservoir temperature is equal to the current reservoir
 263 temperature) the equation can be expressed in linear form (after Archer & Wall (1986)),

$$\frac{P}{z} = \left(-\frac{P_i}{z_i G} \right) G_p + \frac{P_i}{z_i} \quad (2)$$

266 where, P is the reservoir pressure, z is the gas compressibility factor, and the subscript, i ,
 267 denotes initial reservoir conditions.

269 In a true depletion drive reservoir the cumulative volume of produced gas (G_p) will be equal
 270 to the OGIP at $P/z = 0$. Therefore, linear extrapolation of production data on the P/z plot to
 271 the x-axis ($P/z = 0$) provides a reliable estimate of OGIP (see Fig. 5). Likewise, any
 272 estimates of theoretical mass CO_2 storage capacity (an estimate of the maximum volume of
 273 CO_2 that can be stored within a site (Bachu *et al.* 2007)) based on this method should also
 274 yield reliable results.

276 However, difficulties arise in solving the material balance equation in the presence of a water
 277 drive. The majority of gas reservoirs experience some degree of water drive: production
 278 typically induces aquifer influx to the reservoir. The reduction in reservoir pressure (as
 279 production progresses) leads to an expansion of aquifer water resulting in aquifer (water)
 280 influx into the pore space liberated (Dake 1978). The proportion of liberated pore space
 281 occupied by water is dependent on the rate of aquifer influx, or aquifer strength. The
 282 cumulative volume of water influx at reservoir conditions (W_e) is an important parameter
 283 within water drive reservoirs. It gives an indication of aquifer strength and governs reservoir
 284 performance whilst providing a degree of pressure support to the gas reservoir (see Fig. 5).
 285 On a P/z plot, field data will typically deviate from linearity as a result of aquifer influx
 286 (increasing pressure support and W_e) or aquifer depletion (decreasing pressure support and
 287 W_e by fluid transport to another reservoir). As such, the material balance equation (after
 288 Archer & Wall (1986)) becomes:

$$G(B_{gi}) = (G - G_p)B_g + W_e - W_p B_w \quad (3)$$

291 where, W_p is the cumulative volume of produced water and B_w is the water formation volume
 292 factor.

294 Equation 3 can be rearranged as:

296

$$\frac{G_p B_g}{B_g - B_{gi}} = G + \frac{W_e - W_p B_w}{B_g - B_{gi}} \quad (4)$$

298

299

300 Consequently, identification of the reservoir drive mechanism on a P/z plot can be ambiguous
 301 (Vega & Wattenbarger 2000), particularly at the beginning of the productive lifetime of the
 302 reservoir when there is only a small amount of production data available. Despite water drive
 303 reservoirs showing a slightly curved trend across their entire lifetimes on Fig. 5, they could
 304 easily be interpreted to be linear in the initial stages of production leading to misidentification
 305 of the reservoir drive mechanism (i.e. depletion drive rather than water drive). In such cases,
 306 linear extrapolation of data points on the P/z plot will give erroneously high values of OGIP
 307 and hence, will have implications for CO₂ storage capacity estimation (see Fig. 5).

308

309 Data from the four case study reservoirs are presented on P/z plots in Fig. 6. The gas PVT
 310 properties, here and elsewhere in the study, were estimated using the Peng-Robinson
 311 Equation of State (Peng & Robinson 1976), as it allows for accurate estimation of fluid
 312 properties specifically within natural gas reservoirs. The estimated reservoir volumes vary
 313 due to the varying reservoir pressures, which could be well constrained from the regular
 314 measurements, and the temperature which was measured only initially and was therefore kept
 315 constant in the absence of more recent data. In all four cases, data appear to confirm a linear
 316 trend with some reservoirs showing a small amount of fluctuation about the trend. As such,
 317 the reservoir drive mechanism of all four reservoirs was originally considered to be depletion
 318 drive, and linear extrapolation of the datasets to the x-axis provides an estimation of OGIP
 319 (Table 1). This initial interpretation is now checked by re-plotting the same data on a Cole
 320 plot (Pletcher 2002).

321

322 **The Use of Cole Plots to Distinguish Drive Mechanism within a Gas Reservoir and** 323 **Estimate Aquifer Strength**

324

325 The Cole plot (Cole 1969) enables clear distinction between depletion and water drive
 326 reservoirs (Pletcher 2002): depletion drive reservoirs display a positive linear trend, whereas
 327 water drive reservoirs show a curve, and the shape of the curve provides a qualitative
 328 assessment of the strength of the water drive (weak, moderate or strong), (see Fig. 7). As
 329 such, a water drive reservoir is clearly distinguishable from a depletion drive reservoir early
 330 in its productive lifetime. It assumes the expansibility of water is small compared to that of
 331 gas and as such is highly sensitive to the effects of water influx making it a good qualitative
 332 tool. However, it may not be possible to identify aquifer strength until later in the productive
 333 lifetime as the overall shape of the curve needs to be observed. This approach to estimate
 334 aquifer strength within the water drive reservoirs (and therefore the cumulative volume of
 335 water influx, W_e) has been used in the absence of water production data from them.

336

337 The Cole plot (Cole 1969) involves plotting the left hand side of Equation 4, $G_p B_g / (B_g - B_{gi})$,
 338 (the cumulative volume of gas produced at standard conditions multiplied by the gas
 339 formation volume factor divided by the difference between the current and initial gas
 340 formation volume factor), on the y-axis versus the cumulative volume of gas produced, G_p ,
 341 on the x-axis. For depletion drive reservoirs, the term on the far right hand side of Equation
 342 4, $(W_e - W_p B_w) / (B_g - B_{gi})$, (the cumulative volume of water influx minus the cumulative
 343 volume of water produced at the wells multiplied by the water formation volume factor,
 344 divided by the difference between the current and initial gas formation volume factor), goes

345 to zero and the points plot linearly with the y-intercept equal to G (the OGIP). However,
346 within water drive reservoirs, this term is no longer equal to zero and points plot with a
347 curved trend.

348

349 Where a weak water drive is present, $(W_e - W_p B_w)/(B_g - B_{gi})$ decreases with time as the
350 denominator (gas expansion) increases faster than the numerator (net water influx), therefore
351 the resulting plot will have a negative slope that progresses towards the OGIP as production
352 continues (Wang & Teasdale 1987). For moderate and strong water drive, the shape of the
353 curve on the Cole plot is dependent on the gas formation volume factor which, in turn, is
354 dependent on both the cumulative volume of water influx, W_e , and the cumulative volume of
355 produced gas, G_p . In both cases, initially the rate of $G_p B_g/(B_g - B_{gi})$ increases at a decreasing
356 rate. In reservoirs with a strong water drive, this is maintained throughout the productive
357 lifetime resulting in a concave down, increasing curve. However, in reservoirs with a
358 moderate water drive, when the volume of produced hydrocarbons is nearing the volume of
359 the OGIP, $G_p B_g/(B_g - B_{gi})$ begins to decrease at an increasing rate resulting in a concave
360 down curve on the Cole plot across the entire productive lifetime.

361

362 When data from the Hewett Lower Bunter Sandstone reservoir and South Morecambe
363 Sherwood Sandstone reservoir are plotted on a Cole plot, they conform well to an overall
364 linear trend (Fig. 8). Hence, the reservoir drive mechanism is confirmed as depletion drive.
365 The scatter observed on the plot shortly after the onset of production can likely be explained
366 by small errors in pressure measurement (Pletcher 2002). If a pressure gradient existed in the
367 reservoir, wells in different areas will record different pressures under reasonable shut-in
368 times (Payne 1996). Pressure can also be influenced by a well's previous production rate
369 (Payne 1996). This often occurs following the onset of production until the reservoir matures
370 and the production rate stabilises.

371

372 However, when data from the Hewett Upper Bunter Sandstone reservoir and North
373 Morecambe Sandstone reservoir are plotted on a Cole plot a curved trend is observed
374 suggesting the reservoirs experience a degree of water drive (Fig. 8). Data from the Hewett
375 Upper Bunter Sandstone reservoir show that towards the end of the productive lifetime, the
376 curve on the Cole plot appears to decrease, therefore, it is possible to characterise the
377 reservoir drive mechanism as moderate water drive. This is consistent with a water influx
378 ranging between 15 and 50% of the reservoir volume (Hagoort 1988) and is also consistent
379 with the observations of Cooke-Yarborough & Smith (2003) with respect to the reservoir
380 experiencing significant water influx from the Bunter aquifer. Please note, results for the
381 Hewett Upper Bunter Sandstone reservoir does not constitute an Eni interpretation or view.

382

383 Data from the North Morecambe Sherwood Sandstone reservoir fluctuate about the curved
384 trend (Fig. 8). This is partially due to seasonal production from the reservoir. Hence,
385 identification of aquifer strength is not definitive: the reservoir is most likely to have a
386 moderate to strong water drive. As the reservoir is not fully depleted at the limit of the data
387 shown here, it is not possible to observe the presence or absence of the tail-off in the trend
388 which could identify the aquifer strength.

389

390 **Quantifying the Volume of Water Influx into a Gas Reservoir**

391

392 Due to the Hewett Upper Bunter Sandstone reservoir and the North Morecambe Sherwood
393 Sandstone reservoir datasets showing the presence of a water drive when plotted on a Cole
394 plot, it is likely that the OGIP estimated from the P/z plot is an overestimate, as it assumes the

395 reservoir experiences depletion drive only. To check this estimate, Equation 5 (after Dake
396 (1978)) can be used to estimate a value for the cumulative volume of water influx into a
397 reservoir, W_e , in the absence of water production data from the two reservoirs:
398

$$W_e = \frac{G_p - OGIP(1 - E/E_i)}{E} \quad (5)$$

399
400

401 where, G_p is the cumulative volume of produced hydrocarbons, E is the gas expansion factor
402 (the reciprocal of the gas formation volume factor, B_g), and the subscript, i , denotes initial
403 reservoir conditions.

404

405 Within a depletion drive gas reservoir the value of W_e will be zero, or close to it, as there is
406 little or no water encroachment throughout production. However, if a water drive reservoir
407 has been misidentified as a depletion drive reservoir the OGIP may have been overestimated,
408 which would result in an incorrect (negative) value for W_e . Table 2 (a) shows the estimated
409 values of W_e estimated using Equation 5 for the Hewett Upper Bunter Sandstone reservoir
410 and the North Morecambe Sherwood Sandstone reservoir. In both reservoirs, the estimated
411 value of W_e is negative, and therefore there is further evidence to suggest that the OGIP
412 values estimated originally from the P/z plots are incorrect. If both reservoirs experience a
413 water drive as indicated by their respective Cole Plots, their estimated W_e values should be
414 positive, i.e. they should experience aquifer influx as gas is produced from them.

415

416 Aquifer models can be used to estimate W_e , from which a range of OGIP can be estimated.
417 This revised OGIP estimates can then be input to CO₂ storage capacity equations to give a
418 more accurate estimate of CO₂ storage capacity. In this study the unsteady state water influx
419 theory of Van Everdingen and Hurst (1949) was used to estimate the cumulative volume of
420 water influx throughout the productive lifetimes of the Hewett Upper Bunter Sandstone and
421 North Morecambe Sherwood Sandstone reservoirs.

422

423 Aquifers can be classified as radial or linear. The Hewett and Morecambe gas fields share
424 characteristics with both radial and linear aquifer types due to their trap geometries, therefore
425 both radial and linear models were evaluated. Equation 6 can be used to estimate W_e for both
426 a radial aquifer and a linear aquifer:

427

$$W_e = U\Delta PW_D(t_D) \quad (6)$$

428

429 where, U is the aquifer constant, ΔP is the pressure change over the time interval being
430 assessed and $W_D(t_D)$ is the dimensionless cumulative water influx function, after Dake
431 (1978).

432

433 Estimation of the aquifer constant, U , differs for radial and linear aquifers, and is described
434 fully in Dake (1978). Radial aquifers rely upon the estimation of the encroachment angle, f ,
435 using Equation 7 for aquifers which subtend angles of less than 360°, and which can be
436 estimated from the reservoir geometry (see Fig. 9 (a)). The Hewett Upper Bunter Sandstone
437 reservoir is fault bounded to the east by the North Hewett Fault and the South Hewett Fault
438 also runs parallel to the western flank of the anticline, although it is thought not to close the
439 reservoir. This implies flow can occur in a NW-SE orientation (see Fig. 9 (b)). The North
440 Morecambe Sherwood Sandstone reservoir is fault bounded to the east, south and west,

441 therefore the angle of water encroachment into the reservoir is estimated to be 90° from the
 442 north (see Fig. 9 (c)).
 443

$$f = \frac{(\text{encroachment angle})^\circ}{360^\circ} \quad (7)$$

444
 445 For linear aquifers, estimation of the aquifer constant, U, is simpler requiring the width and
 446 length of the aquifer (see Fig. 10). Aquifer length, estimated from the hydraulic diffusivity,
 447 κ_ϕ , (after Wibberley (2002)), was used to evaluate an order-of-magnitude estimate for the
 448 characteristic diffusion distance for a pressure pulse within the water leg to diffuse over a
 449 specified time, based on the pressure depletion history (Figs. 2 and 4), permeability and
 450 porosity data for the reservoirs.
 451

$$\kappa_\phi = \frac{k}{\mu \times \phi \times (c_{res} + c_{fluid})} \quad (8)$$

$$\Delta x = \sqrt{(\kappa_\phi \times \Delta t)} \quad (9)$$

452
 453 where, k is the permeability, μ is the viscosity, ϕ is the porosity, c_{res} is the bulk
 454 compressibility of the matrix, c_{fluid} is the bulk compressibility of the fluid, Δx is the
 455 characteristic diffusion distance and Δt is the characteristic diffusion time.
 456

457 As described previously, a host of porosity and permeability data has been gathered from
 458 multiple wells across the reservoirs which showed a considerable amount of variability.
 459 Conversely, the viscosity and the bulk compressibility of the reservoirs and fluids could be
 460 better constrained. As such, Monte Carlo simulation was used to estimate the hydraulic
 461 diffusivity. This analyses risk for any parameter displaying natural uncertainty through use
 462 of a probability distribution.
 463

464 The results gave a hydraulic diffusivity of 0.026 m²/s in the Hewett Upper Bunter Sandstone
 465 reservoir and 0.012 m²/s in the North Morecambe Sherwood Sandstone reservoir with an
 466 estimated aquifer length of 5.73 km and 1.76 km, respectively.
 467

468 Using the estimates of W_e obtained using the finite radial and linear aquifer models, it is
 469 possible to obtain values of OGIP for both case study reservoirs through rearranging
 470 Equation 5:
 471

$$OGIP = \frac{G_p - W_e E}{1 - E/E_i} \quad (10)$$

472
 473 Results are shown in Table 2 (b), along with the mean W_e values of the radial and linear
 474 aquifer models. It can be seen that OGIP estimates are reduced by a maximum of 1.60 bcm
 475 natural gas in the Hewett Upper Bunter Sandstone reservoir (4.2 %), and by a maximum of
 476 7.26 bcm natural gas in the North Morecambe Sherwood Sandstone reservoir (19.9 %). As
 477 such, this analysis suggests that the OGIP values originally estimated from the P/z plots for
 478 both reservoirs are too large, which can impact CO₂ storage capacity estimates. Please note,
 479 results for the Hewett Upper Bunter Sandstone reservoir does not constitute an Eni
 480 interpretation or view.

481

482 **Importance for Theoretical Mass CO₂ Storage Capacity Estimation**

483

484 Four published theoretical CO₂ storage capacity equations and one effective CO₂ storage
485 capacity equation have been used in this study (Table 3). There are two main approaches to
486 estimating the theoretical CO₂ storage capacity of depleted gas reservoirs. The first approach
487 adapts the geometrically based STOIIP method (stock tank oil initially in place), used
488 frequently in the oil and gas industry to estimate the volume of reserves, for example, the
489 method of Bachu *et al.* (2007) (Table 3, Equation 1). The second approach is based on the
490 principle that a variable proportion of the pore space occupied by the recoverable reserves
491 will be available for CO₂ storage, for example, the methods of Bachu *et al.* (2007), Holloway
492 *et al.* (2006), and Tseng *et al.* (2012) (Table 3, Equations 2, 3 and 4, respectively).

493

494 The effective CO₂ storage capacities of the case study reservoirs were estimated using the
495 method of Tseng *et al.* (2012) (Table 3, Equations 5 and 6). This provides an analytical
496 method for estimation based on material balance and uses parameters that are generally well
497 constrained within depleted gas reservoirs, whether they be depletion drive or water drive
498 reservoirs. Unfortunately, the effective CO₂ storage capacities of the case study reservoirs
499 could not be estimated using the equation of Bachu *et al.* (2007) (Table 3, Equation 7). The
500 method relies upon knowledge of capacity coefficients which are difficult to constrain, there
501 are few published studies that calculate them, and there are no data specifically relating to
502 CO₂ storage in depleted gas reservoirs.

503

504 When estimating both theoretical and effective CO₂ storage capacity, CO₂ density and the gas
505 compressibility factor have been estimated using the Peng-Robinson equation of state (Peng
506 & Robinson 1976), along with the modelling tool, RefProp (Lemmon *et al.* 2013). The
507 results were modelled using the specific natural gas composition of the individual reservoirs
508 and therefore produce well constrained results being governed by the temperature and
509 pressure of the reservoir.

510

511 The gas formation volume factor, B_g , is used to relate the volume of a fluid phase existing at
512 reservoirs conditions of temperature and pressure to its equivalent volume at standard
513 conditions (Archer and Wall 1986). It is equal to the reservoir volume divided by the
514 standard condition volume and relies upon estimation of the gas compressibility factor and as
515 such produces well constrained results.

516

517 Table 4 and Fig. 11 show the estimated theoretical CO₂ storage capacities of the four
518 reservoirs calculated using the original estimated values for OGIP. The water drive
519 reservoirs (Hewett Upper Bunter and North Morecambe Sherwood Sandstone) have
520 additional results based on the W_e and OGIP estimates from the radial and linear aquifer
521 modelling, and also an average of the two models. From Table 4, theoretical estimates vary
522 by 16 % in the Hewett Lower Bunter reservoir, 81 % in the Hewett Upper Bunter reservoir,
523 88 % in the South Morecambe reservoir and 91 % in the North Morecambe reservoir
524 (percentage difference between the highest and lowest estimates, based on average aquifer
525 models in the water drive reservoirs).

526

527 It can be seen from the results using the geometric method of Bachu *et al.* (2007) (Table 3,
528 Equation 1), the theoretical CO₂ storage capacities of the water drive reservoirs are increased
529 when the OGIP is estimated via aquifer modelling. This is even more apparent in Fig. 12
530 which shows the percentage difference between the theoretical CO₂ storage capacity

531 estimates in the water drive reservoirs compared to those estimated originally, represented by
532 the dashed line (zero difference). Fig. 12 shows that the storage capacities may have been
533 originally *under-estimated* using original OGIPs by approximately 4 % in the Hewett Upper
534 Bunter Sandstone reservoir, and approximately 30 % in the North Morecambe Sherwood
535 Sandstone reservoir using the geometric method of Bachu *et al.* (2007). It is also only this
536 equation that is susceptible to variation as a result of the aquifer modelling, as can be seen in
537 Fig. 12. The methods of Bachu *et al.* (2007), Equation 2, Holloway *et al.* (2006) and Tseng
538 *et al.* (2012) result in the same storage capacity estimates in each reservoir, and therefore
539 show 0 % difference on Fig. 12.

540

541 Overall, the methods of Bachu *et al.* (2007) (Table 3, Equation 2), Holloway *et al.* (2006) and
542 Tseng *et al.* (2012) produce consistent, conservative estimates for CO₂ storage capacities in
543 both the depletion drive and water drive reservoirs (see Fig. 12), and provide a good basis
544 from which effective CO₂ storage capacities can be estimated.

545

546 All of the theoretical CO₂ storage capacity equations rely on either direct estimation of the
547 OGIP, or the estimation of a parameter that relies upon the OGIP (such as the recovery
548 factor), apart from the method of Tseng *et al.* (2012) (Table 3, Equation 4). Therefore, it is
549 important to obtain a precise value for the OGIP so that estimated CO₂ storage capacities are
550 more accurate. This study has shown that aquifer modelling can help avoid over-estimation
551 of the OGIP in water drive reservoirs and give more accurate values of W_e to be input into
552 storage capacity equations (i.e. positive values). However, there are alternative published
553 methods such as Bachu *et al.* (2007) (Table 3, Equation 2), and Tseng *et al.* (2012) which do
554 not require this level of detail. The theoretical method of Tseng *et al.* (2012) completely
555 avoids use of the OGIP or any dependent variables, and is not influenced by aquifer
556 modelling since it avoids use of W_e (Fig. 12), whilst producing conservative, consistent
557 capacity estimates (Fig. 11). The method of Bachu *et al.* (2007) (Table 3, Equation 2),
558 appears to give similar results despite it being possible to use incorrect OGIP values and
559 dependent variables; as such, the method should be used with caution.

560

561 The geometric method of Bachu *et al.* (2007) (Table 3, Equation 1), produces the greatest
562 capacity estimates and is the method most susceptible to variability. The method is over-
563 simplified as gross reservoir volume is defined by only area and height: parameters that are
564 difficult to quantify as individual values. The method can yield comparable results to the
565 alternative theoretical methods in thin reservoirs (as is the case for the Hewett Lower Bunter
566 Sandstone reservoir (see Fig. 11)). However, in thicker reservoirs it is assumed the whole
567 thickness of the reservoir is entirely gas-bearing (particularly problematic in the Morecambe
568 gas fields which consist of illite-affected parts of the reservoir over a substantial thickness,
569 and also with them being thick, dipping reservoirs meaning the gas-bearing volume is prism-
570 shaped not box-shaped (Fig. 11)). As such, it will always over-estimate the true gross rock
571 volume. A second issue with the method is that the cumulative volumes of injected and
572 produced water are often not measured (as this is not necessary for successful production
573 from gas reservoirs in most cases), therefore any estimated values are likely to be incorrect.
574 A final issue is the value used for water saturation: it is often assessed prior to production, but
575 the value is likely to change as production progresses, particularly in water drive reservoirs,
576 and is not often re-assessed.

577

578 The alternative theoretical methods of Bachu *et al.* (2007) (Table 3, Equation 2), Holloway *et al.*
579 *et al.* (2006) and Tseng *et al.* (2012), generally predict comparable results and rely upon input
580 parameters which can be well constrained, including initial pressures and temperatures within

581 the gas reservoirs. However, this study has demonstrated that the values of parameters such
582 as the OGIP, which is generally considered to be well constrained, should not necessarily be
583 taken at face value. The Hewett Upper Bunter and North Morecambe reservoirs, originally
584 modelled as depletion drive reservoirs, have original OGIP values that are over-estimates.
585 Therefore, it is imperative to ascertain whether a proposed storage reservoir experiences a
586 water drive. If the OGIP is over-estimated it follows that the final theoretical CO₂ storage
587 capacity estimates may be erroneous.

588
589 Fig. 13 shows the effective CO₂ storage capacity results from all four reservoirs and have
590 been estimated using the method of Tseng *et al.* (2012) (Table 3, Equation 5), based on the
591 original OGIP estimates. The water drive reservoirs have additional results from aquifer
592 modelling. The bars on Fig. 13 represent the theoretical CO₂ storage capacity estimates from
593 the method of Tseng *et al.* (2012) (Table 3, Equation 4). The effective capacity is, by
594 definition, a subset (reduction) of the theoretical capacity and, in most cases here, the
595 effective CO₂ storage capacity estimate is less than the corresponding theoretical estimate.
596 The effective capacity of the Hewett Upper Bunter Sandstone reservoir based on the original
597 OGIP values is greater than the theoretical capacity estimate and is further evidence that the
598 original OGIP values are incorrect. Following aquifer modelling, the results from the water
599 drive reservoirs seem more in-line with expected results. In general, the effective capacities
600 are between 64 – 86 % of theoretical capacities within the depletion drive reservoirs, and 53 –
601 79 % within the water drive reservoirs.

602
603 The effective CO₂ storage capacity method of Tseng *et al.* (2012) (Table 3, Equation 5 and
604 6), requires the cumulative volume of water influx into a reservoir, W_e , across the productive
605 lifetime of a gas reservoir to be known. This parameter is especially sensitive to the
606 estimated OGIP value, therefore it is paramount this value is precise to obtain accurate
607 effective CO₂ storage capacity estimates in water drive gas reservoirs. This can be achieved
608 through aquifer modelling as this study has shown. Within depletion drive reservoirs the
609 value of W_e will be zero or negligible. All other required parameters for this method are
610 generally well constrained, including the cumulative volume of produced hydrocarbons
611 which is constantly measured being the saleable asset.

612 613 **Conclusions**

614 This study has shown that theoretical CO₂ storage capacity estimates vary as a result of
615 several factors: (a) the reservoir drive mechanism (or degree of aquifer support a reservoir
616 receives, (b) the method of storage capacity estimation used, and (c) the degree of natural
617 variability of input parameters and/or overall accuracy of the input parameters.

618
619 The difficulties in solving the material balance equation in the presence of a water drive have
620 been demonstrated here. Cole plots can provide a more definitive way of characterising the
621 reservoir drive mechanism as any deviation from a linear trend on the Cole plot denotes the
622 presence of a water drive.

623
624 It is important to establish the correct reservoir drive mechanism so that more precise
625 estimates of OGIP, and any dependent variables can be input into theoretical and effective
626 CO₂ storage capacity equations. Establishing a precise estimate of OGIP, on which the
627 estimation of W_e relies, is of particular importance for effective CO₂ storage capacity
628 estimation. Imprecise values can result in capacity being erroneously estimated. Aquifer
629 modelling can be used to increase the precision of the OGIP estimates and their dependent

630 variables, however, the resulting storage capacity estimate inevitably depends on the method
631 being used.

632

633 The geometric theoretical CO₂ storage capacity method of Bachu *et al.* (2007) (Table 3,
634 Equation 1), consists of parameters which are over-simplistic for the treatment of individual
635 gas fields and as such can result in considerable over-estimates of CO₂ storage capacity. The
636 alternative theoretical methods of Bachu *et al.* (2007) (Table 3, Equation 2), Holloway *et al.*
637 (2006), and Tseng *et al.* (2012) generally predict comparable results and rely on input
638 parameters that can be well constrained with little variability. The theoretical method of
639 Tseng *et al.* (2012) was found to give reliable estimates as it avoids input of the OGIP, or any
640 dependent variables, however, aquifer modelling can be used to produce consistent,
641 conservative theoretical CO₂ storage capacity results via the methods of Bachu *et al.* (2007)
642 and Holloway *et al.* (2006).

643

644 Overall, theoretical CO₂ storage capacity estimates vary by 16 % in the Hewett Lower Bunter
645 reservoir, 81 % in the Hewett Upper Bunter reservoir, 88 % in the South Morecambe
646 reservoir and 91 % in the North Morecambe reservoir (percentage difference between the
647 highest and lowest estimates, based on average aquifer models in the water drive reservoirs).
648 Comparing the theoretical capacity estimates of Tseng *et al.* (2012) with the effective method
649 of the same author, estimated effective capacities are between 64 – 86 % of theoretical
650 capacities within the depletion drive reservoirs, and 53 – 79 % within the water drive
651 reservoirs.

652

653 Our acknowledgements go to Eni Hewett Ltd., operator of the Hewett Unit assets, and their partner,
654 Perenco UK (Gas) Ltd., for providing access to historic production and pressure data relating to the
655 Hewett Unit gas fields. Our acknowledgements also go to Centrica, operator of the South and North
656 Morecambe assets, for providing historic production and pressure data relating to the Morecambe gas
657 fields. Please note that all interpretations made in the study, unless specifically stated, are those of the
658 authors and do not necessarily reflect the views of Eni Hewett Ltd., Perenco UK (Gas) Ltd., or
659 Centrica. Similarly, previously published data used in the calculations and results for the Hewett
660 reservoirs do not constitute an Eni Hewett Ltd. interpretation or view. ALC would like to
661 acknowledge funding by NERC (NERC Open CASE studentship to Durham University, grant
662 reference NE/G011222/1). JI is part-funded by the Royal Society (Royal Society Industry Fellowship
663 with Badley Geoscience Ltd. and Geospatial Research Ltd.). ALC would like to take this opportunity
664 to thank her CASE partners, IHS and Badley Geoscience Ltd., for the provision of data, training and
665 guidance during her research on the Hewett and Morecambe Gas Fields.

666

667 **References**

668 AGARWAL, R.G., AL-HUSSAINY, R. & RAMEY H. J., J. 1965. The Importance of Water Influx
669 in Gas Reservoirs. *Journal of Petroleum Technology*, **17**, 1336–1342.

670 ARCHER, J.S. & WALL, C.G. 1986. *Petroleum Engineering : Principles and Practice*.
671 London, Graham & Trotman.

672 BACHU, S., BONIJOLY, D., BRADSHAW, J., BURRUSS, R., HOLLOWAY, S., CHRISTENSEN, N.P.
673 & MATHIASSEN, O.M. 2007. CO₂ storage capacity estimation: Methodology and gaps.
674 *International Journal of Greenhouse Gas Control*, **1**, 430–443.

675 BASTIN, J.C., BOYCOTT-BROWN, T., SIMS, A. & WOODHOUSE, R. 2003. The South
676 Morecambe Gas Field, Blocks 110/2a, 110/3a, 110/7a and 110/8a, East Irish Sea.
677 *Geological Society, London, Memoirs*, **20**, 107–118, doi:
678 10.1144/gsl.mem.2003.020.01.09.

679 BENTHAM, M. 2006. *An Assessment of Carbon Sequestration Potential in the UK - Southern*
680 *North Sea Case Study*.

- 681 BROOK, M., SHAW, K., VINCENT, C. & HOLLOWAY, S. 2003. Gestco case study 2a-1: Storage
682 Potential of the Bunter Sandstone in the UK sector of the Southern North Sea and the
683 adjacent onshore area of Eastern England. *BGS Commissioned Report CR/03/154N*, 1–
684 44.
- 685 BRUNS, J.R., FETKOVICH, M.J. & MEITZEN, V.C. 1965. The Effect of Water Influx on p/z-
686 Cumulative Gas Production Curves. *Journal of Petroleum Technology*, **17**, 287–291.
- 687 CHIERICI, G.L., PIZZI, G. & CIUCCI, G.M. 1967. Water Drive Gas Reservoirs: Uncertainty in
688 Reserves from Past History. *Journal of Petroleum Technology*, **19**, 237–244.
- 689 CLARKE, A., IMBER, J., DAVIES, R., YIELDING, G., HEAFFORD, A., DANIELS, S., van HUNEN,
690 J. & MATHIAS, S. 2010. Hewett: A Promising Carbon Storage Site? Presented at the
691 Petroleum Geoscience Research Collaboration Showcase, London, 23-24 November.
- 692 COLE, F.W. 1969. *Reservoir Engineering Manual*. Houston, Gulf Publishing Co.
- 693 COOKE-YARBOROUGH, P. & SMITH, E. 2003. The Hewett Fields: Blocks 48/28a, 48/29,
694 48/30, 52/4a, 52/5a, UK North Sea: Hewett, Deborah, Big Dotty, Little Dotty, Della,
695 Dawn and Delilah Fields. *Geological Society, London, Memoirs*, **20**, 731–739, doi:
696 10.1144/gsl.mem.2003.020.01.60.
- 697 COWAN, G. & BOYCOTT-BROWN, T. 2003. The North Morecambe Field, Block 110/2a, East
698 Irish Sea. *Geological Society, London, Memoirs*, **20**, 97–105, doi:
699 10.1144/gsl.mem.2003.020.01.08.
- 700 DAKE, L.P. 1978. *Fundamentals of Reservoir Engineering*. Amsterdam, Elsevier Scientific
701 Publishing Co.
- 702 GLOBAL CCS INSTITUTE. 2015. *The Global Status of CCS 2015*.
- 703 HAGOORT, J. 1988. Chapter 11: Natural Depletion. In: Hagoort, J. (ed.) *Developments in*
704 *Petroleum Science*. New York, Elsevier Science Publishing Company, 233–261., doi:
705 10.1016/s0376-7361(09)70333-4.
- 706 HOLLOWAY, S. 2009. Storage capacity and containment issues for carbon dioxide capture and
707 geological storage on the UK continental shelf. *Proceedings of the Institution of*
708 *Mechanical Engineers, Part A: Journal of Power and Energy*, **223**, 239–248.
- 709 HOLLOWAY, S., VINCENT, C.J. & KIRK, K.L. 2006. *Industrial Carbon Dioxide Emissions and*
710 *Carbon Dioxide Storage Potential in the UK*.
- 711 JACKSON, D.I., JACKSON, A.A., EVANS, D., WINGFIELD, R.T.R., BARNES, R.P. & ARTHUR,
712 M.J. 1995. *The Geology of the Irish Sea*. Balogh Scientific Books, British Geological
713 Survey Series United Kingdom offshore regional report.
- 714 JOHNSON, H., WARRINGTON, G. & STOKER, S.J. 1994. 6. Permian and Triassic of the
715 Southern North Sea. In: Knox, R. W. O. & Cordey, W. G. (eds) *Lithostratigraphic*
716 *Nomenclature of the UK North Sea*. British Geological Survey, Nottingham.
- 717 KIRK, K.L. 2006. *Potential for Storage of Carbon Dioxide in the Rocks Beneath the East*
718 *Irish Sea*.
- 719 LEMMON, E.W., HUBER, M.L. & MCLINDEN, M.O. 2013. NIST Standard Reference Database
720 23: Reference Fluid Thermodynamic and Transport Properties - REFPROP.
- 721 PAYNE, D.A. 1996. Material-balance calculations in tight-gas reservoirs: The pitfalls of p/z
722 plots and a more accurate technique. *SPE Reservoir Engineering*, **11**, 260–267.
- 723 PENG, D.-Y. & ROBINSON, D.B. 1976. A New Two-Constant Equation of State. *Industrial &*
724 *Engineering Chemistry Fundamentals*, **15**, 59–64, doi: 10.1021/i160057a011.
- 725 PLETCHER, J.L. 2002. Improvements to Reservoir Material-Balance Methods. *SPE Reservoir*
726 *Evaluation & Engineering*, **5**, 49–59.
- 727 STUART, I.A. 1993. The geology of the North Morecambe Gas Field, East Irish Sea Basin.
728 *Geological Society, London, Petroleum Geology Conference series*, **4**, 883–895, doi:
729 10.1144/0040883.
- 730 STUART, I.A. & COWAN, G. 1991. The South Morecambe Field, Blocks 110/2a, 110/3a,

731 110/8a, UK East Irish Sea. *Geological Society, London, Memoirs*, **14**, 527–541, doi:
732 10.1144/gsl.mem.1991.014.01.66.

733 TSENG, C.-C., HSIEH, B.-Z., HU, S.-T. & LIN, Z.-S. 2012. Analytical approach for estimating
734 CO₂ storage capacity of produced gas reservoirs with or without a water drive.
735 *International Journal of Greenhouse Gas Control*, **9**, 254–261, doi:
736 <http://dx.doi.org/10.1016/j.ijggc.2012.04.002>.

737 VAN EVERDINGEN, A.F. & HURST, W. 1949. The Application of the Laplace Transformation
738 to Flow Problems in Reservoirs. *Journal of Petroleum Technology*, **1**, 305–324.

739 VEGA, L. & WATTENBARGER, R.A. 2000. New Approach for Simultaneous Determination of
740 the OGIP and Aquifer Performance with No Prior Knowledge of Aquifer Properties and
741 Geometry. *Society of Petroleum Engineers*.

742 WANG, B. & TEASDALE, T.S. 1987. GASWAT-PC: A microcomputer program for gas
743 material balance with water influx. *Society of Petroleum Engineers*, 25–42.

744 WARRINGTON, G., AUDLEY-CHARLES, M.G., ET AL. 1980. *A Correlation of Triassic Rocks in*
745 *the British Isles*. Special Report of the Geological Society of London, No. 13.

746 WIBBERLEY, C.A.J. (2002). Hydraulic Diffusivity of Fault Gouge Zones and Implications for
747 Thermal Pressurisation during Seismic Slip. *Earth Planets Space*, **54**, 1153-1171.

748

749

750 **Figure Captions**

751

752 **Fig. 1.** *Location, structure and areal extent of the gas fields of the Hewett Unit, Southern*
753 *North Sea. The limit of the areal extent is defined by the original gas-water contact within*
754 *each reservoir prior to production, or fault closure of the traps. Modified from Cooke-*
755 *Yarborough and Smith (2003).*

756

757 **Fig. 2.** *Location, structure and areal extent of the South and North Morecambe Gas Fields of*
758 *the East Irish Sea Basin. The limit of the areal extent is defined by the original gas-water*
759 *contact within each reservoir prior to production, or fault closure of the traps. Modified*
760 *from Jackson et al. (1995).*

761

762 **Fig. 3.** *Production and pressure data for the Hewett Upper and Lower Bunter Sandstone*
763 *reservoirs and the Little Dotty Upper Bunter Sandstone reservoir. The dashed lines indicate*
764 *the dates when the reservoirs came online.*

765

766 **Fig. 4.** *Production and pressure data for the North Morecambe and South Morecambe*
767 *Sherwood Sandstone reservoirs.*

768

769 **Fig. 5.** *Material balance (P/z) plot showing major trends depending on the degree of aquifer*
770 *influx into a reservoir assuming all pressure support to the producing reservoir is a result of*
771 *aquifer influx. Modified from Hagoort (1988).*

772

773 **Fig. 6.** *P/z plots of the four reservoirs: Hewett Lower Bunter Sandstone, Hewett Upper*
774 *Bunter Sandstone, South Morecambe Sherwood Sandstone and North Morecambe Sherwood*
775 *Sandstone. All four reservoirs have been interpreted as having a depletion drive reservoir*
776 *mechanism based on the linear trends of the plots indicated by the red dashed lines. Please*
777 *note, results for the Hewett reservoirs do not constitute an Eni interpretation or view.*

778 **Fig. 7.** *Major trends on a Cole Plot. Cole plots can provide a clearer distinction between*
779 *water drive and depletion drive reservoirs than a P/z plot as any degree of water influx into a*
780 *reservoir produces a curve on the Cole plot. The overall shape of the curve indicates aquifer*
781 *strength. Redrawn from Pletcher (2002).*

782

783 **Fig. 8.** *Cole plots of the four reservoirs: Hewett Lower Bunter Sandstone, Hewett Upper*
784 *Bunter Sandstone, South Morecambe Sherwood Sandstone and North Morecambe Sherwood*
785 *Sandstone. The Hewett Lower Bunter Sandstone and South Morecambe Sherwood Sandstone*
786 *reservoirs have been confirmed to have a depletion drive reservoir mechanism, whereas the*
787 *Hewett Upper Bunter Sandstone and North Morecambe Sherwood Sandstone reservoirs show*
788 *a moderate water drive when their data is plotted on the Cole plot. Please note, results for*
789 *the Hewett reservoirs do not constitute an Eni interpretation or view.*

790

791 **Fig. 9.** *Radial aquifer geometry (a) schematic, redrawn from Dake (1978), (b) the Hewett*
792 *Upper Bunter Sandstone reservoir, and (c) the North Morecambe Sherwood Sandstone*
793 *reservoir. The reservoir outlines in (b) and (c) can be observed with the bounding faults in*
794 *red. In (b) the encroachment angle is 180° with water influx from both the north-west and*
795 *south-east. In (c) the encroachment angle is 90° with water influx from the north. Please*
796 *note, results for the Hewett Upper Bunter Sandstone reservoir does not constitute an Eni*
797 *interpretation or view.*

798 **Fig. 10.** *Linear aquifer geometry schematic, redrawn from Dake (1978).*

799

800 **Fig. 11.** *Theoretical CO₂ Storage Capacity of the four reservoirs: Hewett Lower Bunter (HLB), South Morecambe (SM), Hewett Upper Bunter (HUB) and North Morecambe (NM). The capacities of all four reservoirs have been calculated using the originally estimated values for OGIP. The two water drive reservoirs (HUB and NM) also have estimates based on radial and linear aquifer modelling, and an average of the two models. Please note, results for the Hewett Upper Bunter Sandstone reservoir does not constitute an Eni interpretation or view.*

806

807 **Fig. 12.** *Graph of percentage difference of theoretical CO₂ storage capacity estimates between estimates using the original OGIP values and revised OGIP estimates following aquifer modelling. The black dashed line indicates the base-line, i.e. no difference between estimates. Please note, results for the Hewett Upper Bunter Sandstone reservoir do not constitute an Eni interpretation or view.*

813 **Fig. 13.** *Effective CO₂ Storage Capacity of the four reservoirs based on the method of Tseng et al. (2012): Hewett Lower Bunter (HLB), South Morecambe (SM), Hewett Upper Bunter (HUB) and North Morecambe (NM). The capacities of all four reservoirs have been calculated using the originally estimated values for OGIP. The two water drive reservoirs (HUB and NM) also have estimates based on radial and linear aquifer modelling, and an average of the two models. The bars represent the theoretical CO₂ storage capacity estimates using the theoretical method of Tseng et al. (2012). Please note, results for the Hewett reservoirs do not constitute an Eni interpretation or view.*

820

821 **Table 1.** *Estimates of original gas in place based upon Cooke-Yarborough & Smith (2003)*
822 *for the Hewett reservoirs, and extrapolation of a linear trend on P/z plots of reservoir data*
823 *for the South Morecambe and North Morecambe gas fields (shown in Fig. 4)*

| RESERVOIR | OGIP (bcm) |
|---------------------------------------|------------|
| HEWETT LOWER BUNTER SANDSTONE | 59.5 |
| HEWETT UPPER BUNTER SANDSTONE | 38.4 |
| SOUTH MORECAMBE SHERWOOD SANDSTONE | 155.7 |
| NORTH MORECAMBE SHERWOOD SANDSTONE | 36.5 |

824

825

826 **Table 2.** (a) Estimates of W_e based on the original estimated values for OGIP (original gas in
827 place) for the Hewett Upper Bunter Sandstone (Cooke-Yarborough & Smith 2003) and North
828 Morecambe Sherwood Sandstone (P/z plots in Fig. 4), assuming they are depletion drive
829 reservoirs, using Equation 1. (b) Estimates of original gas in place (OGIP) using Equation
830 10, based on mean W_e values (cumulative volume of water influx into a reservoir) from
831 aquifer models. Please note, results for the Hewett Upper Bunter Sandstone reservoir do not
832 constitute an Eni interpretation or view.

| | | HEWETT UPPER BUNTER | | NORTH MORECAMBE | |
|-----|---|-------------------------|------------------------|-------------------------|------------------------|
| | | W_e (m ³) | OGIP (m ³) | W_e (m ³) | OGIP (m ³) |
| (a) | ESTIMATED W_e BASED ON INDUSTRY ESTIMATE OGIP | -2.153E+08 | 3.840E+10 | -6.745E+07 | 3.653E+10 |
| (b) | FINITE RADIAL AQUIFER MEAN | 1.700E+07 | 3.680E+10 | 1.820E+07 | 2.927E+10 |
| | FINITE LINEAR AQUIFER MEAN | 4.190E+06 | 3.689E+10 | 1.560E+07 | 2.949E+10 |
| | MEAN OF RADIAL AND LINEAR MODELS | 1.060E+07 | 3.685E+10 | 1.690E+07 | 2.938E+10 |

834 **Table 3.** *Published theoretical and effective CO₂ storage capacity equations for depleted gas*
 835 *reservoirs. See Table 5 for explanation of parameters.*

| STORAGE CAPACITY EQUATION | AUTHOR | EQUATION NUMBER |
|--|-------------------------------|-----------------|
| THEORETICAL CO ₂ STORAGE CAPACITY EQUATIONS | | |
| $M_{CO_2t} = \rho_{CO_2r} [R_f Ah \phi (1 - S_w) - V_{iw} + V_{pw}]$ | Bachu <i>et al.</i> (2007) | 1 |
| $M_{CO_2t} = \rho_{CO_2r} R_f (1 - F_{IG}) OGIP \left[\frac{(P_s Z_r T_r)}{(P_r Z_s T_s)} \right]$ | Bachu <i>et al.</i> (2007) | 2 |
| $M_{CO_2t} = \left(\frac{V_{GAS}[stp]}{B_{igas}} \times \rho_{CO_2r} \right)$ | Holloway <i>et al.</i> (2006) | 3 |
| $M_{CO_2t} = \frac{\rho_{CO_2r} (G_{phc} \times B_{gas})}{B_{iCO_2}} = \frac{\rho_{CO_2r} (G_{phc} \times z_{gas})}{z_{iCO_2}}$ | Tseng <i>et al.</i> (2012) | 4 |
| EFFECTIVE CO ₂ STORAGE CAPACITY EQUATIONS | | |
| $M_{injCO_2} = \rho_{CO_2r} \times G_{injCO_2}$ | Tseng <i>et al.</i> (2012) | 5 |
| where, | | |
| $G_{injCO_2} = G_{phc} - G_{ihc} + \frac{P_{reshc/CO_2}}{z_{reshc/CO_2}} \left(\frac{z_{ihc}}{P_{ihc}} G_{ihc} - W_e \frac{T_{sc}}{P_{sc} T} \right)$ | Tseng <i>et al.</i> (2012) | 6 |
| $M_{CO_2e} = C_m C_b C_h C_w C_a M_{CO_2t} \equiv C_e M_{CO_2t}$ | Bachu <i>et al.</i> (2007) | 7 |

837 **Table 4.** *Estimated theoretical mass CO₂ storage capacities of the four reservoirs. All*
 838 *reservoir capacities have been calculated using the original estimated values for OGIP. The*
 839 *two water drive reservoirs (Hewett Upper Bunter Sandstone and North Morecambe*
 840 *Sherwood Sandstone) also have estimates based on radial and linear aquifer modelling, and*
 841 *an average of the two models. Please note, results for the Hewett reservoirs do not constitute*
 842 *an Eni interpretation or view.*

| | DEPLETION DRIVE RESERVOIRS | | WATER DRIVE RESERVOIRS | |
|-------------------------------|----------------------------|-----------------|------------------------|-----------------|
| | HEWETT LOWER BUNTER | SOUTH MORECAMBE | HEWETT UPPER BUNTER | NORTH MORECAMBE |
| TSENG ET AL. 2012 | | | | |
| Industry | 2.81E+08 | 3.26E+08 | 1.78E+08 | 1.55E+08 |
| Radial | | | 1.78E+08 | 1.55E+08 |
| Linear | | | 1.78E+08 | 1.55E+08 |
| Average | | | 1.78E+08 | 1.55E+08 |
| BACHU ET AL. 2007, EQUATION 1 | | | | |
| Industry | 2.49E+08 | 2.53E+09 | 7.94E+08 | 8.20E+08 |
| Radial | | | 8.27E+08 | 1.07E+09 |
| Linear | | | 8.26E+08 | 1.06E+09 |
| Average | | | 8.26E+08 | 1.07E+09 |
| BACHU ET AL. 2007, EQUATION 2 | | | | |
| Industry | 2.43E+08 | 3.12E+08 | 1.55E+08 | 1.03E+08 |
| Radial | | | 1.55E+08 | 1.03E+08 |
| Linear | | | 1.55E+08 | 1.03E+08 |
| Average | | | 1.55E+08 | 1.03E+08 |
| HOLLOWAY ET AL. 2006 | | | | |
| Industry | 2.35E+08 | 3.07E+08 | 1.57E+08 | 1.00E+08 |
| Radial | | | 1.57E+08 | 9.99E+07 |
| Linear | | | 1.57E+08 | 9.99E+07 |
| Average | | | 1.57E+08 | 9.99E+07 |

843

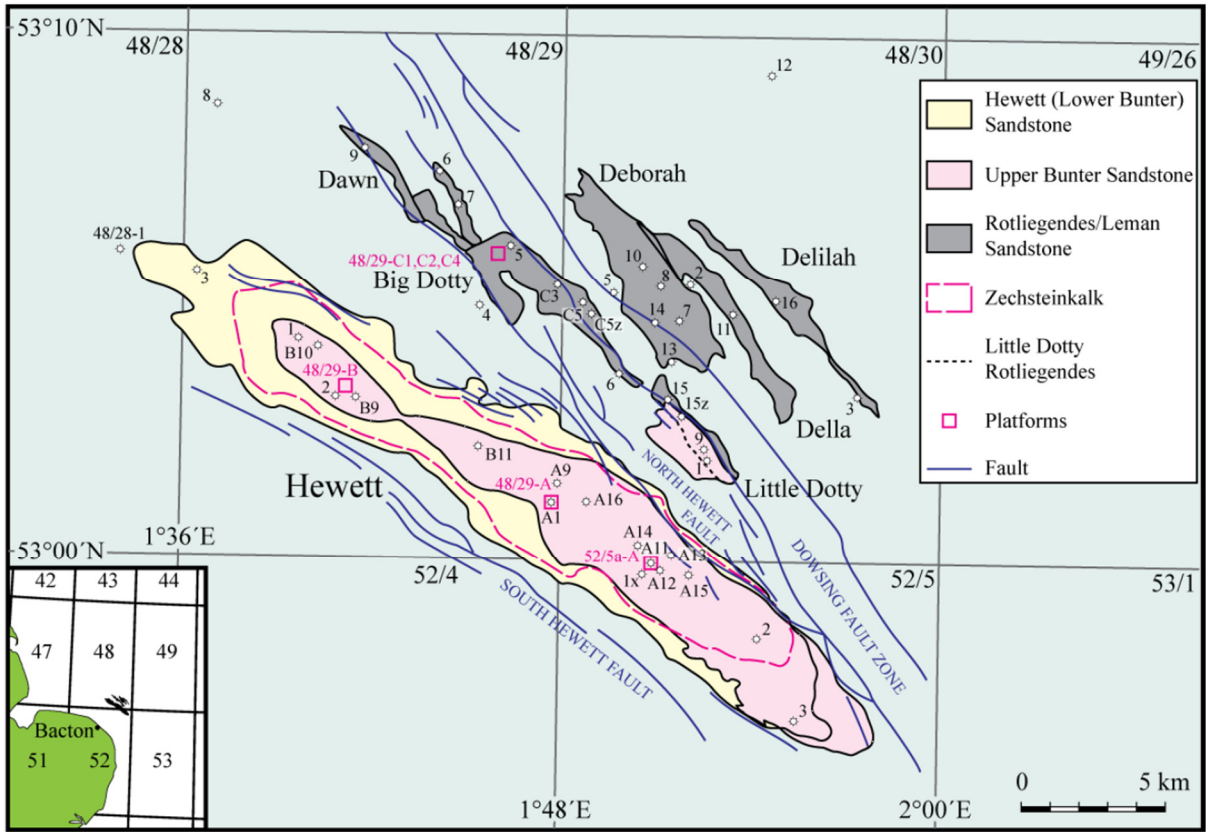
844
845

Table 5. *Table of nomenclature for Theoretical and Effective Storage Capacity Equations (Table 3).*

| ABBREVIATION | DEFINITION | UNITS |
|------------------|--|-------------------|
| ϕ | Reservoir porosity | Dimensionless |
| ρ_{CO_2r} | Density of carbon dioxide at reservoir conditions | kg/m ³ |
| A | Reservoir/play area | m ² |
| B_{gas} | Reservoir gas formation volume factor at end of production | Dimensionless |
| B_{iCO_2} | CO ₂ formation volume factor at initial reservoir conditions | Dimensionless |
| B_{igas} | Gas formation volume factor at initial reservoir conditions | Dimensionless |
| C_a | Capacity coefficient for aquifer strength | Dimensionless |
| C_b | Capacity coefficient for buoyancy | Dimensionless |
| C_e | Effective capacity coefficient | Dimensionless |
| C_h | Capacity coefficient for heterogeneity | Dimensionless |
| C_m | Capacity coefficient for mobility | Dimensionless |
| C_w | Capacity coefficient for water saturation | Dimensionless |
| E | Gas expansion factor | Dimensionless |
| F_{IG} | Fraction of injected gas | Dimensionless |
| G_{ihc} | Volume of initial hydrocarbons | m ³ |
| G_{injCO_2} | Cumulative volume of injected CO ₂ | m ³ |
| G_{phc} | Volume of produced hydrocarbons | m ³ |
| h | Reservoir height/thickness | m |
| M_{CO_2e} | Effective mass storage capacity for CO ₂ | tonnes |
| M_{CO_2t} | Theoretical mass storage capacity for CO ₂ | tonnes |
| M_{injCO_2} | Effective mass storage capacity for injected CO ₂ | tonnes |
| OGIP | Original gas in place | m ³ |
| P_{ihc} | Pressure at initial reservoir conditions | Pa |
| P_r | Reservoir pressure | Pa |
| P_{reshc/CO_2} | Pressure of residual hydrocarbon/CO ₂ mix | Pa |
| P_s | Surface pressure | Pa |
| P_{sc} | Pressure at standard conditions | Pa |
| R_f | Recovery factor | Dimensionless |
| S_w | Water saturation | Dimensionless |
| T | Reservoir temperature | Kelvin |
| T_r | Reservoir temperature | Kelvin |
| T_s | Surface temperature | Kelvin |
| T_{sc} | Temperature at standard conditions | Kelvin |
| V_{GAS} | Volume of ultimate recoverable reserves | m ³ |
| V_{iw} | Volume of injected water | m ³ |
| V_{pw} | Volume of produced water | m ³ |
| W_e | Cumulative volume of water influx into a reservoir | m ³ |
| Z_{gas} | Reservoir gas compressibility factor at end of production | Dimensionless |
| Z_{iCO_2} | CO ₂ gas compressibility factor at initial reservoir conditions | Dimensionless |
| Z_{ihc} | Gas compressibility factor at initial reservoir conditions | Dimensionless |
| Z_r | Reservoir compressibility | Dimensionless |
| Z_{reshc/CO_2} | Gas compressibility factor of residual hydrocarbon/CO ₂ mix | Dimensionless |
| Z_s | Surface compressibility | Dimensionless |

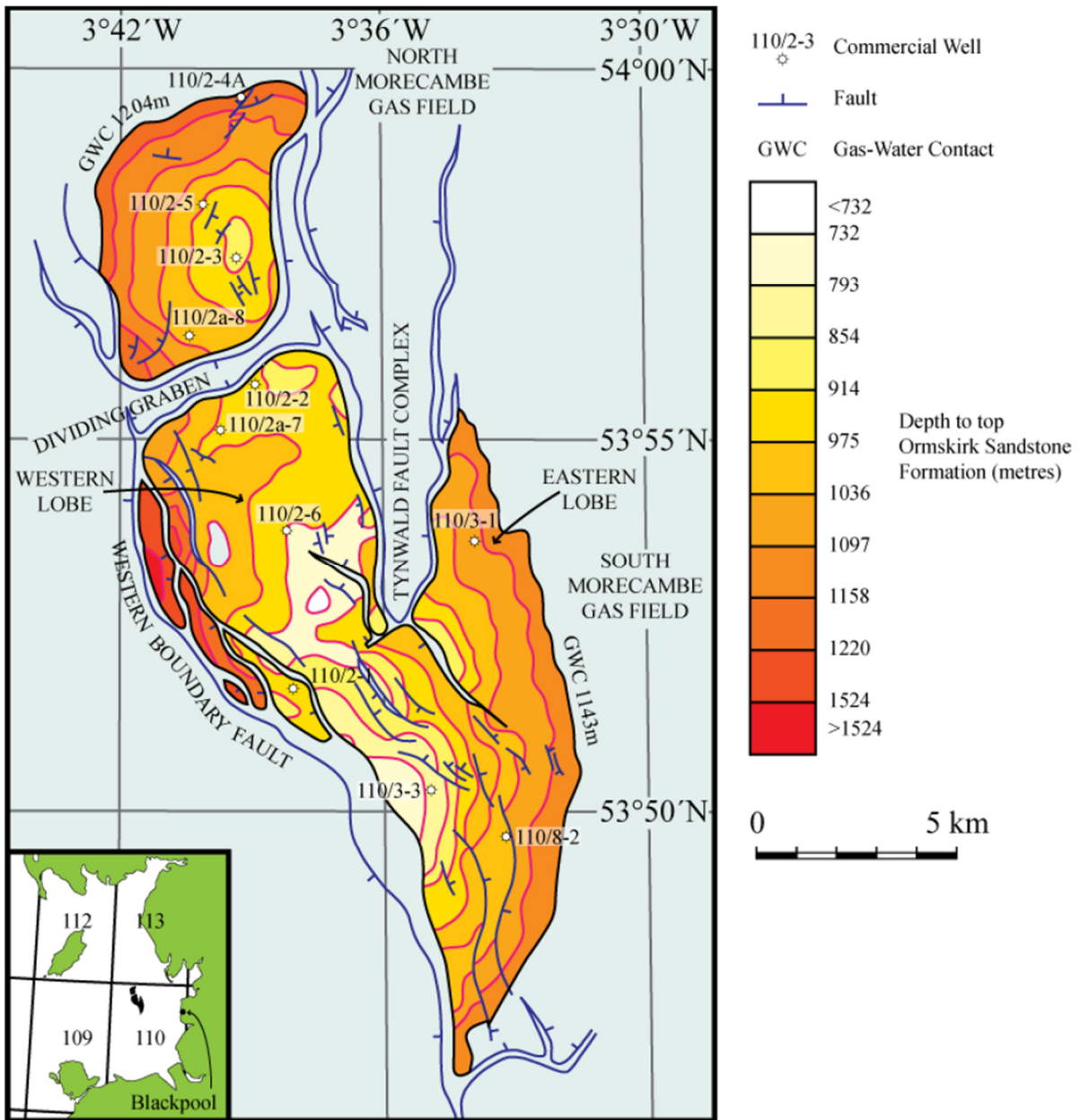
846

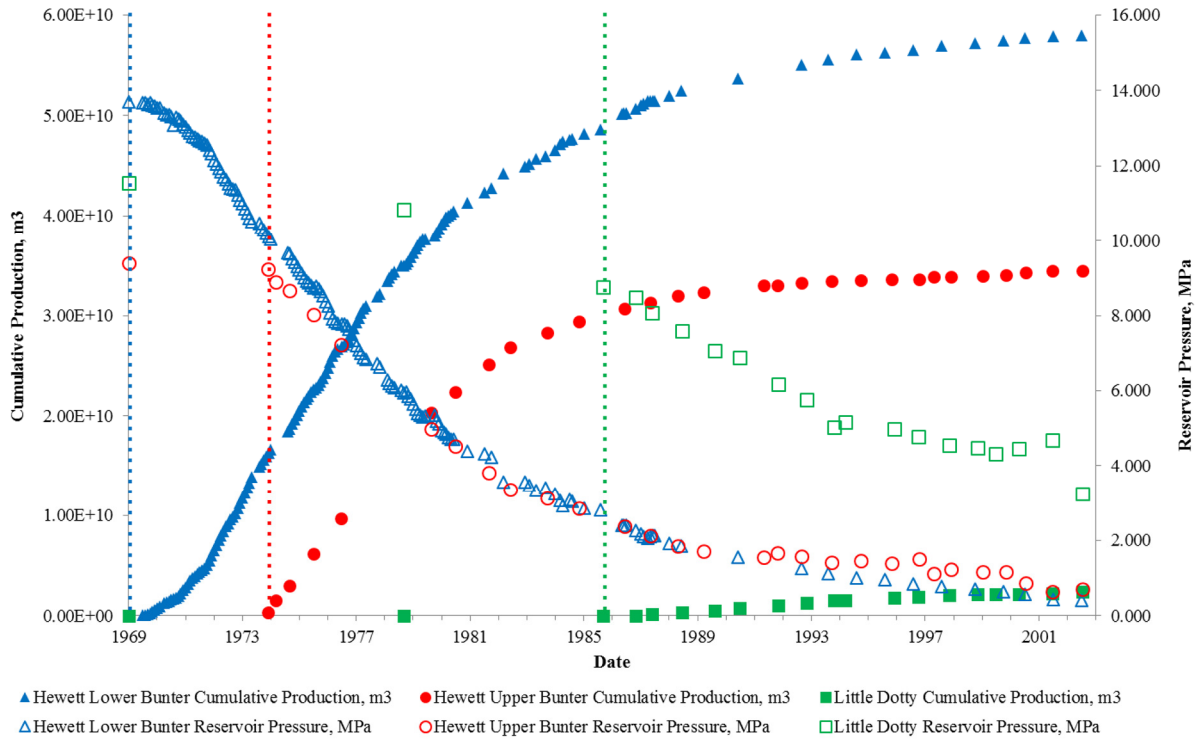
847



848

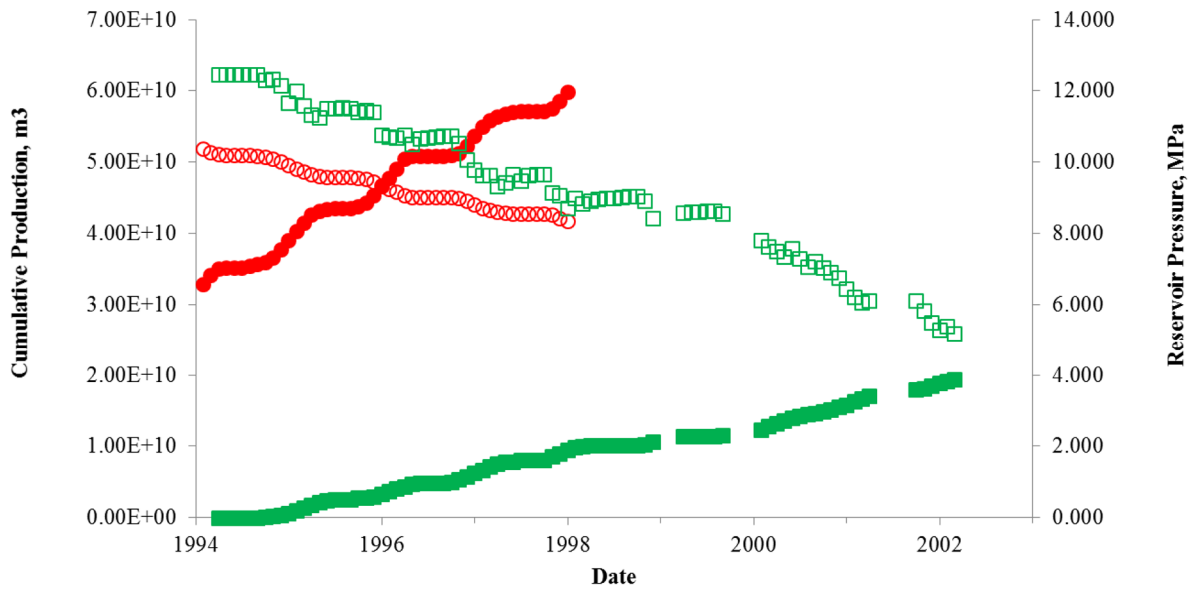
849





853

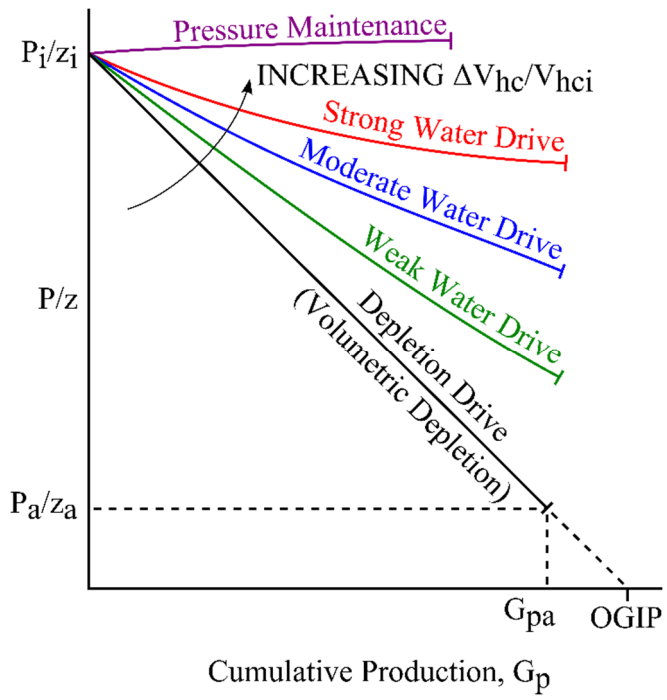
854



- South Morecambe Cumulative Production, m3
- South Morecambe Reservoir Pressure, MPa
- North Morecambe Cumulative Production, m3
- North Morecambe Reservoir Pressure, MPa

855

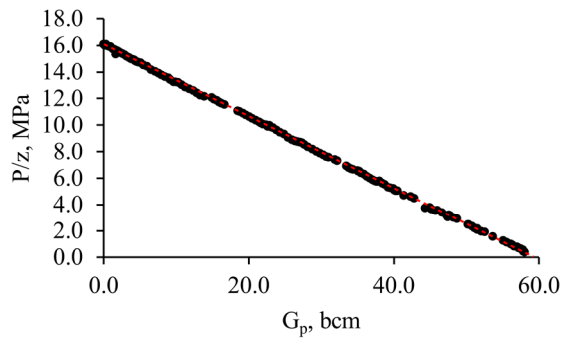
856



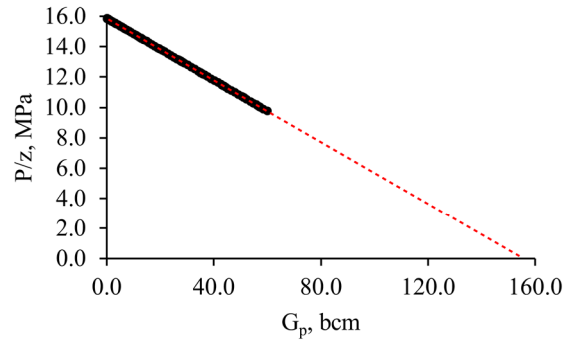
857

858

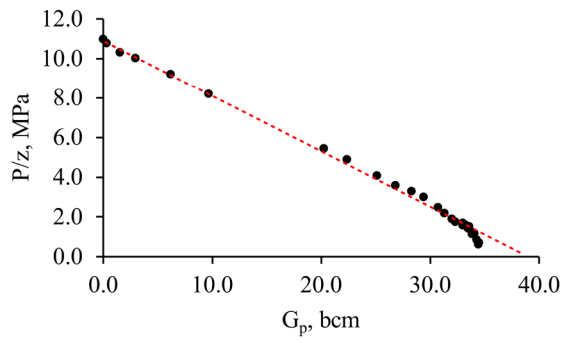
Hewett Lower Bunter Sandstone



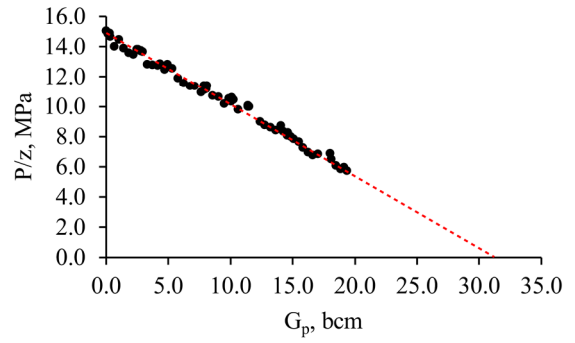
South Morecambe Sherwood Sandstone



Hewett Upper Bunter Sandstone

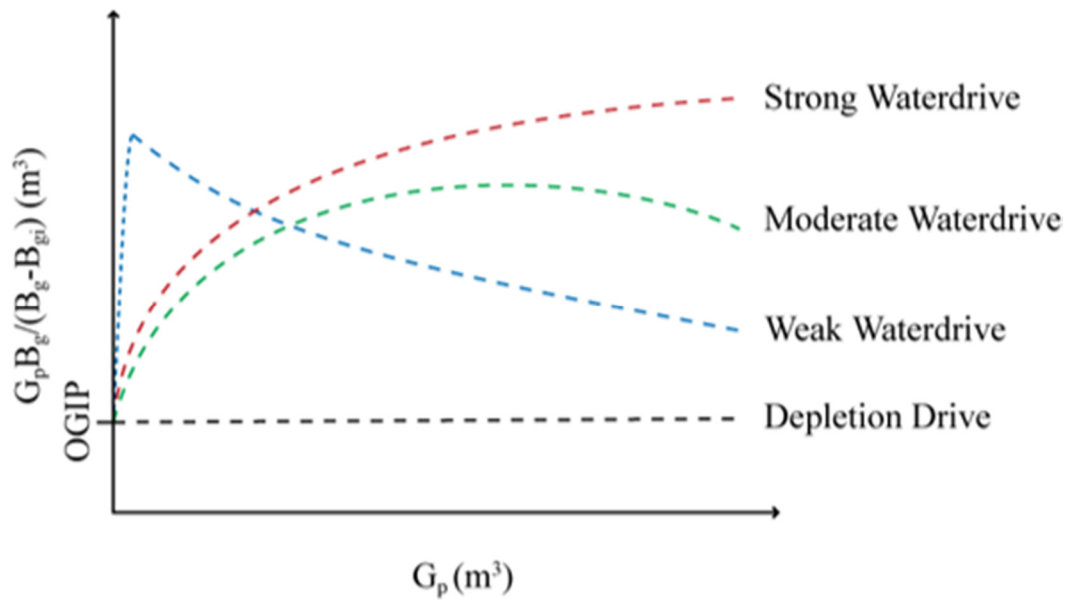


North Morecambe Sherwood Sandstone



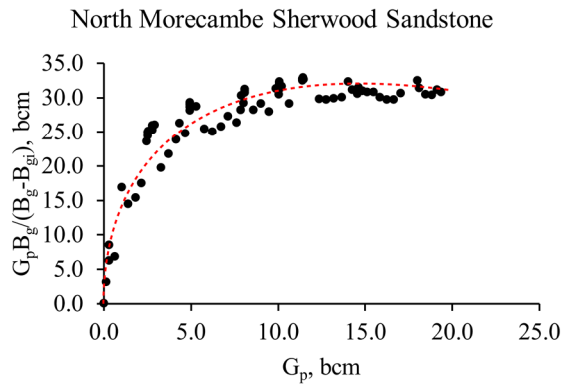
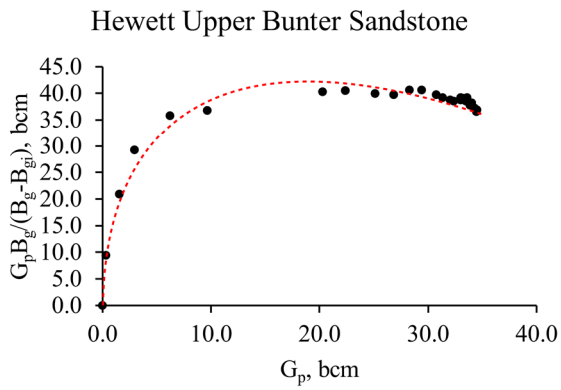
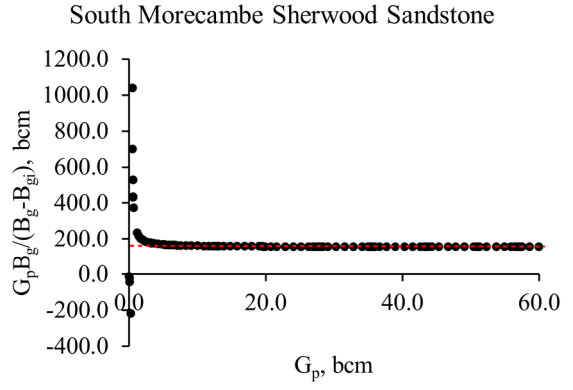
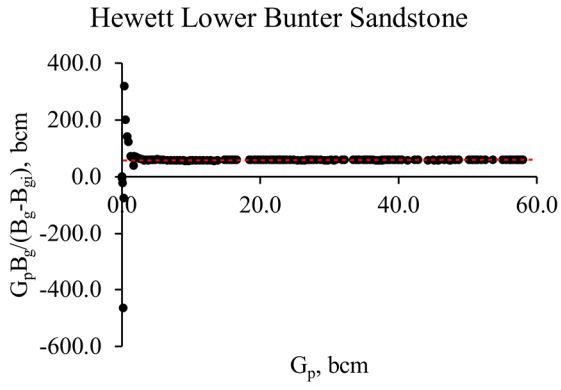
859

860



861

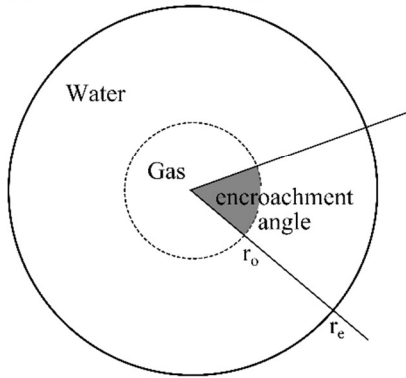
862



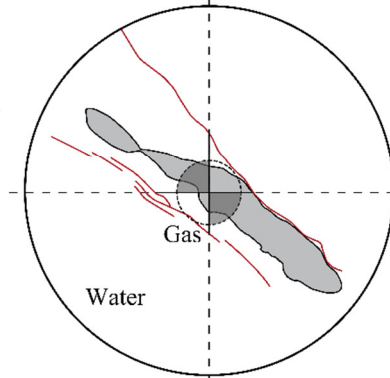
863

864

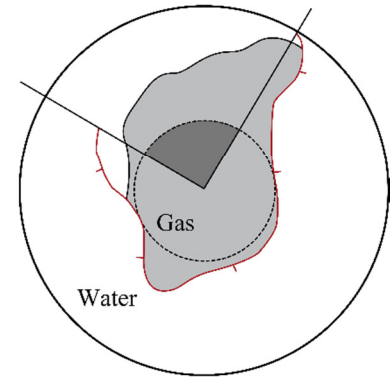
(a) $f = (\text{encroachment angle})^\circ / 360^\circ$



(b) encroachment angle = 180°

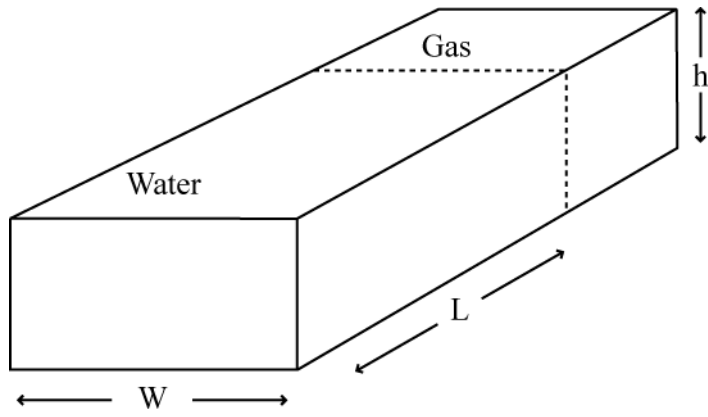


(c) encroachment angle = 90°



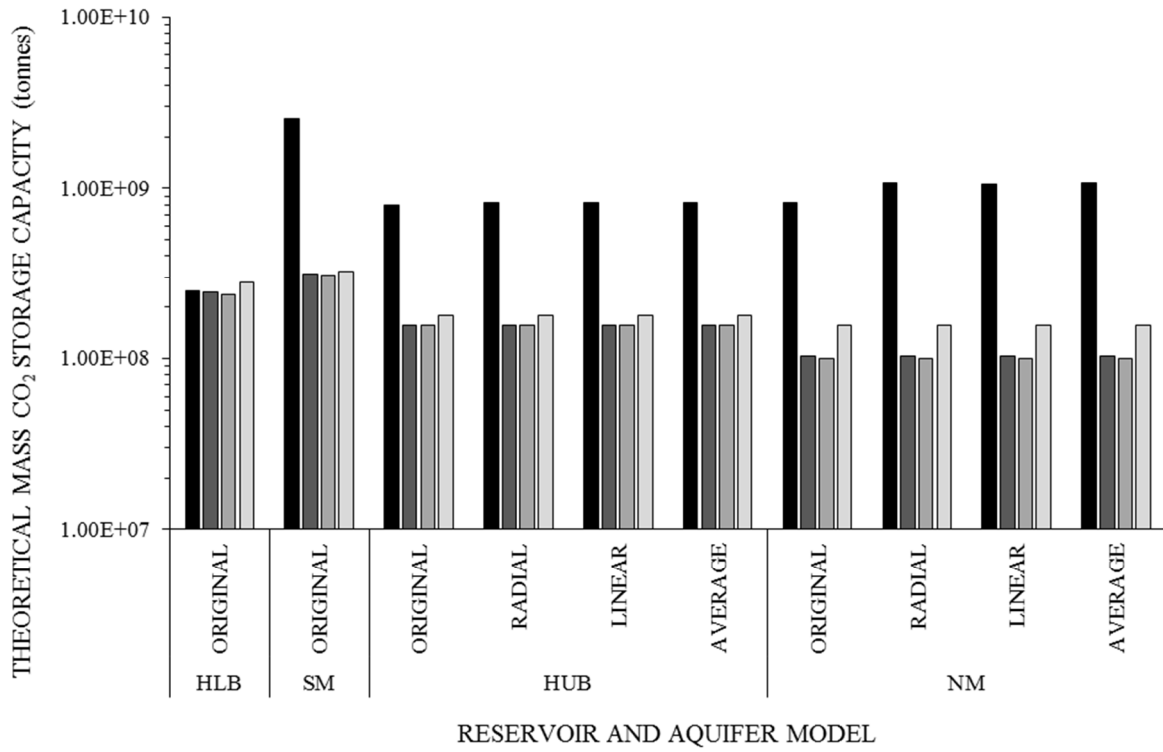
865

866



867

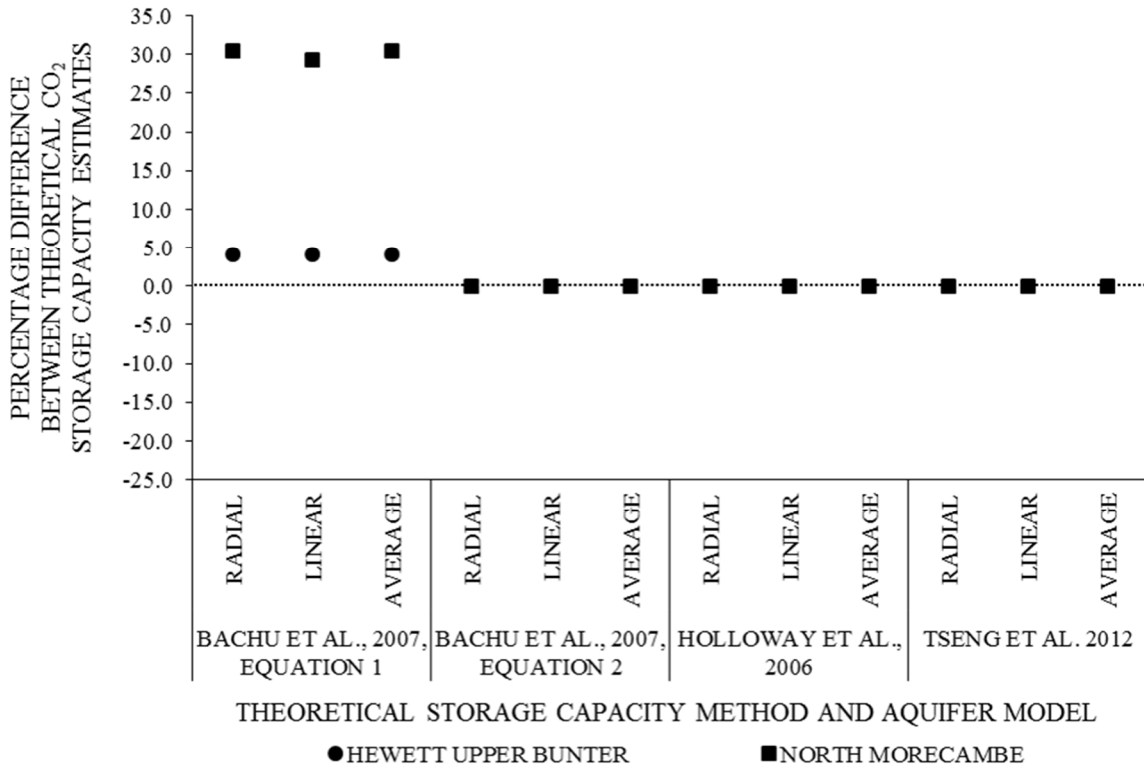
868



- BACHU ET AL., 2007, EQUATION 1
- BACHU ET AL., 2007, EQUATION 2
- ▒ HOLLOWAY ET AL., 2006
- TSENG ET AL., 2012

869

870



871

872

